Available online at www.eccomasproceedia.org
Eccomas Proceedia SMART (2023) 1423-1434

ECCOMAS
Proceedia

X ECCOMAS Thematic Conference on Smart Structures and Materials
SMART 2023
D.A. Saravanos, A. Benjeddou, N. Chrysochoidis and T. Theodosiou (Eds)

TRIBOLOGICAL STUDY OF A NEW SELF-EXPANDING NITINOL STENT DEDICATED TO THE TREATMENT OF VENOUS STENOSIS

Achref Sallami*[1,2], Pierrick Malecot[3,4], Fabrice Richard[1], Michaël Fontaine[3], Arnaud Lejeune[1], Sébastien David[2], Paul Vescovo[2], Christophe Moureaux[2], and Philippe Stempflé[3]

[1] Université de Franche-Comté, CNRS, institut FEMTO-ST, F-25000 Besançon, France
e-mail: achref.sallami@femto-st.fr - Web page: https://www.femto-st.fr/en

[2] Cisteo MEDICAL, 1 rue Anne de Pardieu, 25000 Besançon, France
e-mail: asallami@cisteomedical.com - Web page: https://www.cisteomedical.com/en

[3] SUPMICROTECH, CNRS, institut FEMTO-ST, F-25000 Besançon, France

[4] Université de Bretagne Sud, CNRS, IRDL, F-56100 Lorient, France

Key words: Self-expanding nitinol stent; Frictional behaviour law; X-ray tomography; Optical topography; Contact mechanics theory

Abstract. One aspect of current research on self-expanding super-elastic nitinol stents is mainly focused on the development of a new design, which itself depends on the human venous and arterial systems to be treated. In this context, the present study focuses on a one-piece double cross-sectional stent used in the treatment of venous stenosis, affecting the vena cava, iliac veins and their bifurcations. During stent placement, many tribological problems occur when the stent slides in the guide-wire (catheter), mainly due to the lack of knowledge about their frictional behaviour. Among this lack of information, the level of contact pressure - related to the unknown real contact area between the compressed stent and the polytetrafluoroethylene (PTFE) catheter - is largely misunderstood.

The aim of this work is to describe a method allowing to determine both the contact pressure and the evolution of the real contact area during sliding movement using a multi-scale approach involving (*i*) X-ray tomography at the macroscopic scale for determining the static contact pressure, and (*ii*) a 3D optical measurement instrument at the microscopic scale coupled with the Persson's theory to calculate the evolution of the real contact areas. The latter takes into account both (*i*) the elastic properties of each material, and (*ii*) the variations of the topographic parameters with contact pressures, and (*iii*) the sliding parameters (ie, velocities and sliding distance).

These results lead to a better prediction of the true frictional behaviour between the nitinol stent and the PTFE catheter. In addition, the methodology allows to simplify the complex numerical simulation of a real stent sliding within a catheter by an equivalent model using a much more simplified geometry including the frictional behaviour of the complex stent.

1 Introduction

Among the most well known shape memory alloys (SMAs) are those based on Ni-Ti, copper and iron [1]. These alloys have the ability to remember and recover their original shapes against significant externally applied loads and exhibit a solid-to-solid, reversible phase transformation. The applications of SMAs are very diverse, ranging from mechanical engineering to medicine, etc.

Peer-review under responsibility of the organizing committee of SMART 2023.
doi: 10.7712/150123.9914.444643

Ni-Ti based SMAs are the most usable in the medical field. These SMAs are known as nitinol, The term nitinol derives from its composition and the place of its discovery (Nickel Titanium Naval Ordnance Laboratory). Nitinol exhibits two important behaviours: *i* a shape memory effect (SME) and *ii* a superelastic behaviour (SE), Whether nitinol is superelastic or has a shape memory behaviour depends on alloy composition and heat treatment, in addition to the method of fabrication.. In the topic of this paper, only the SE behaviour is suitable for our application. During large deformations, nitinol is subjected to an isothermal reversible phase transformation from austenite to martensite which induces the SE behaviour. As martensite is metastable, it returns to the austenitic state if the stress is released and regains its initial shape [2, 3].

Medical applications of nitinol include round orthodontic bows, endodontic rotary files, stents etc. In this context, the present study focuses on a one-piece double cross-sectional stent used in the treatment of venous stenosis, affecting the vena cava, iliac veins and their bifurcations (cf. Fig.1a and Fig.1b). Superelastic nitinol stents are structures that are placed in arteries or veins by catheterization. For this purpose, polytetrafluoroethylene (PTFE) is commonly used as a catheter owing to its low friction and good biocompatibility. Because a stent is a large object, its section must be reduced into a wire form to be inserted within the PTFE catheter. Once positioned in the diseased vein or artery , it returns to its shape on its own, taking advantage of the SE behaviour - without any use of a balloon as needed for stainless steel stents- to expand the diseased vein [4] (cf. Fig.1c).

The aims of this paper is to enhance our knowledge about the release force, which is strongly dependent on the tribological behaviour of the nitinol stent within the PTFE catheter. First, the frictional behavior of a nitinol tube and a nitinol stent inside a PTFE catheter will be investigated using a tensile testing machine in Sections 3.1 and 3.2, consecutively. Second, the evolution of the real contact area will be computed by integrating both, the materials part of the friction dissipation and the effect of the stent topography using a multiscale approach combining X-Ray tomography and optical topography (section 3.3). Third, the evolution of the tangential stress at the interface between stent and PTFE catheter will be computed in traction and compression at various velocities. Since this tangential stress integrates both, *(i)* the stent design and, *(ii)* the materials behaviours, it is likely to be used to simplify the numerical model computing the releasing force assessment.

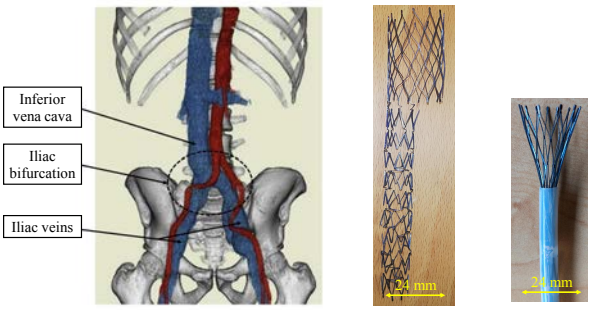

Figure 1: (a) Image characterizing the inferior vena cava, the two iliac veins and the iliac bifurcation of the venous system [5]; (b) Design of the auto-expansible stent; (c) Snapshot of stent release from PTFE catheter

2 Materials and methods

2.1 Tribological setup

Experiments have been carried out on two kinds of nitinol samples: *(i)* a tube of ASTM F-2063 bio-medical nitinol tube (inner diameter "Φ_{ID}": 4.1 mm, outer diameter "Φ_{OD}": 5 mm, wall thickness

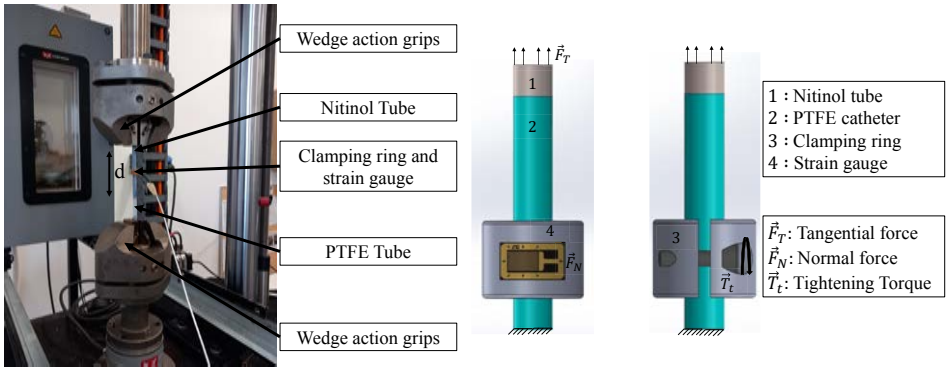

(a) (b)

Figure 2: (a) Tensile testing machine equipped for nitinol tube/PTFE catheter tribological test ; (b) The normal load is applied by means of a clamping ring equipped by a strain gauge. During traction or compression the nitinol tube is pulled or pushed by the movable head with respect to the PFTE catheter clamped at the fixed head

"w_t": 0.45 mm) and, *(ii)* a laser-cut stent from an ASTM F-2063 bio-medical nitinol displaying a suitable design for the aforementioned medical application. The latter has been thermally treated as reported in our previous work [6]. In order to simulate the stent release, the two samples have been forced to rub within a PTFE catheter (Φ_{ID}: 5 mm, Φ_{OD}: 6 mm, w_t: 0.5 mm) by means of a tensile testing machine (Instron Electropuls E 10000) as shown in figure 2a. The capacity of the machine is $\pm$ 1 KN on loading. Materials properties are compiled in Table 1.

Table 1: Elastic properties of Nitinol and PTFE

	Nitinol	PTFE
E (MPa)	28230	1200
ν	0.33	0.46

In the case of the nitinol tube, an accurate normal pressure is applied on the nitinol/PTFE assembly with a torque screw controlled by a strain gauge glued on the clamping ring (cf. Fig.2b). Tensile test gives the evolution of the pulling/pushing forces as a function of the displacement for various normal loads – checked by the strain gauge – and imposed velocities. The maximum displacement is d=$\pm$10 mm - either pulling or pushing - and testing velocities are 100, 500, and 1000 μm.s^{-1}, respectively. For each velocity, three clamping forces have been imposed: 5.163, 8.625, and 15.327 N, respectively. The tangential force F_T is quantified by the load cell of the tensile testing machine. All tests have been carried out at room temperature and ambient environment.

In the case of the stent, the normal pressure is, only, imposed by its radial expansion force on the PTFE catheter because of its SE behaviour, as shown in figure 3. In these configurations, pulling or pushing forces are directly connected to the tangential forces induced by traction or compression of nitinol samples within the PTFE catheter.

2.2 Topographical analysis

Stent surface topography has been carried out by using a digital microscope KEYENCE VHX-5000 (cf. Fig.4). All topographical analyses leading to the real contact area have been made using the free SPM data analysis software Gwyddion (http://gwyddion.net/) following a specific procedure which will

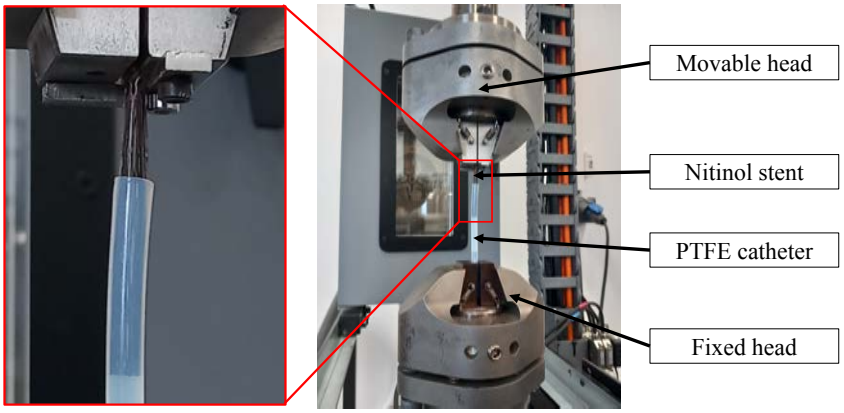

Figure 3: Tensile testing machine equipped for nitinol stent/PTFE catheter tribological test. During traction or compression the nitinol stent is pulled or pushed by the movable head with respect to the PFTE catheter clamped at the fixed head. Normal pressure is here only imposed by the radial expansion force of the nitinol stent on the PTFE catheter

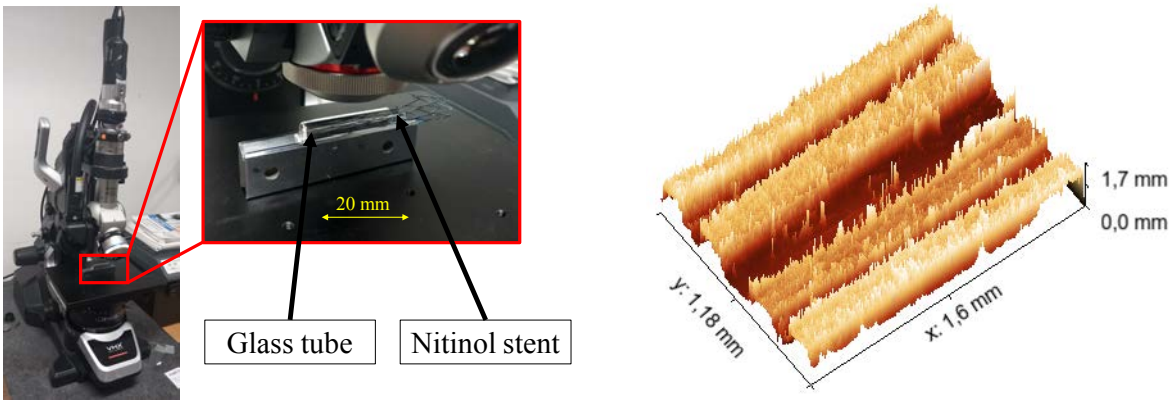

(a) (b)

Figure 4: (a) Digital microscope KEYENCE VHX-5000 enabling to characterize the topography of the stent within a tube ; (b) 3D topographical view of the stent compressed within a glass tube showing the different stent strands

be described in section 3.3.

2.3 X-RAY Tomography

X-ray SOLUTION EASYTOM tomographic equipment (Tube voltage=116 keV, Tube current=102μA) has been used to determine the mean contact pressure imposed by the compressed stent within the PTFE catheter, as shown in figure 5. For this purpose, image analysis has been done with VGstudio max software using a Filtered Back-projection algorithm based on grey level thresholds for image reconstruction [7].

3 Results and discussion

3.1 Tribological behaviour of nitinol tube within PTFE catheter

Figures 6a and 6b show the typical evolution of the pulling (Fig.6a) and pushing (Fig.6b) force versus displacement assessed when the nitinol tube is rubbing within the PTFE catheter at 100 μms^{-1}. These

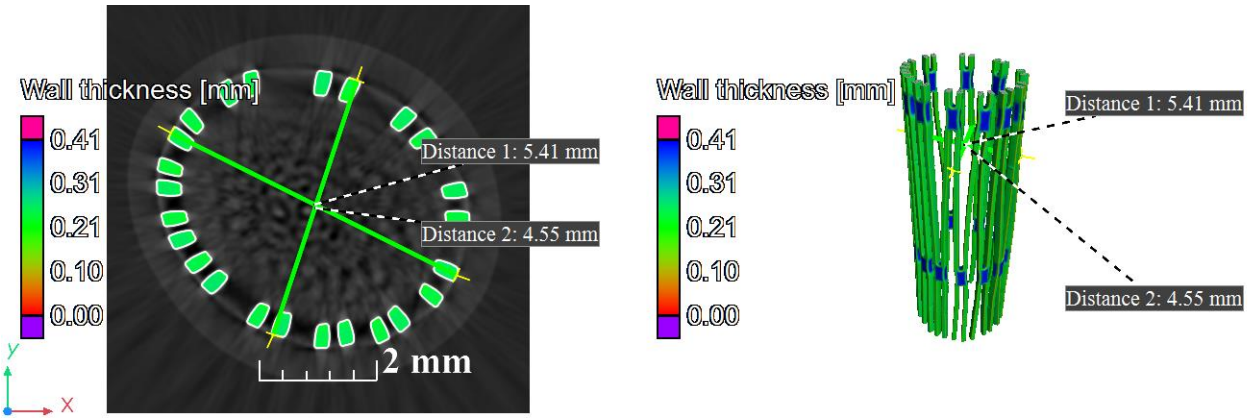

(a) (b)

Figure 5: Tomographical analysis of the nitinol stent within the PTFE catheter : (a) top view revealing the deformation of the nitinol stent within the PTFE catheter and corresponding (b) 3D view

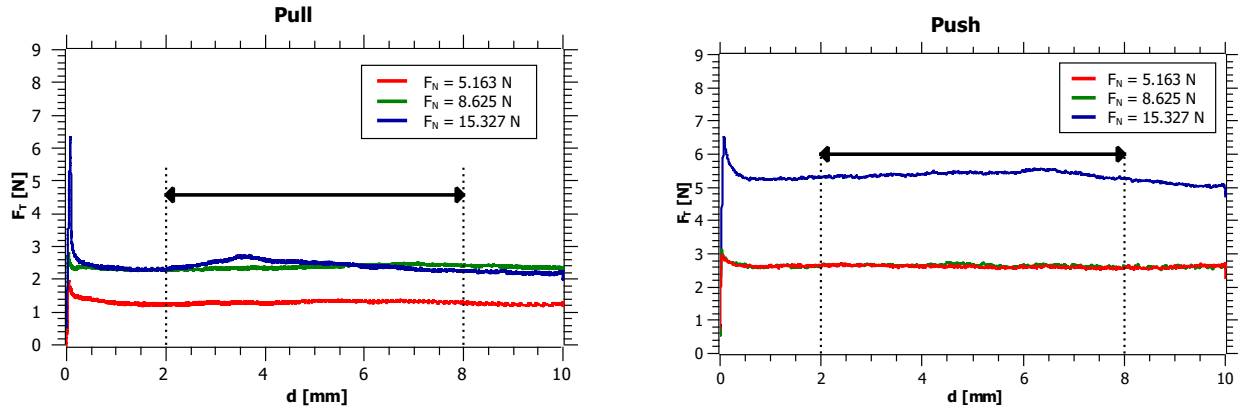

(a) (b)

Figure 6: Evolution of the tangential force occurring between the nitinol tube and the PTFE catheter versus displacement in (a) traction (pull) and in (b) compression (push) at 100 μms^{-1} (smoothed with a 20 points adjacent averaging algorithm)

actually correspond to the tangential forces induced by the frictional behaviour in traction and compression for different normal forces imposed by the torque screw. Evaluation of the tangential force within the steady zone – i.e., arrows in between 2 and 8 *mm* on Fig.6a and 6b – allows us to compute the dynamic coefficient of friction by using the so-called Coulomb's friction relationship (i.e., $\mu = \frac{F_T}{F_N}$), with F_N being assessed by the strain gauge. Figure 7 shows the average coefficient of friction of the nitinol/PTFE couple computed for tests in traction and compression for all velocities and normal loads. It appears that the coefficient of friction in traction and compression is quite stable when considering their standard deviations. Their values are around 0.29 and 0.34 in traction and compression, respectively. The latter only take into account the materials properties because of the good quality of the nitinol tube surface.

3.2 Tribological behaviour of nitinol stent within PTFE catheter

Figures 8a and 8b show the evolution of the pulling (Fig.8a) and pushing (Fig.8b) force versus displacement assessed when the nitinol stent is rubbing within the PTFE catheter for three different velocities. It is worth noting that frictional behaviours are more noisy compared to the ones previously

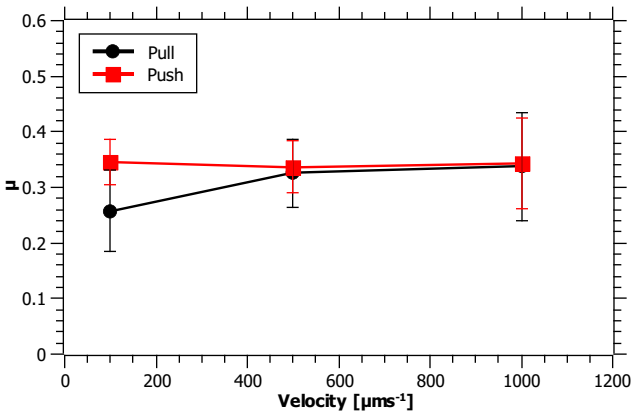

Figure 7: Evolution of the average coefficient of friction versus sliding velocities for pulling and pushing tests

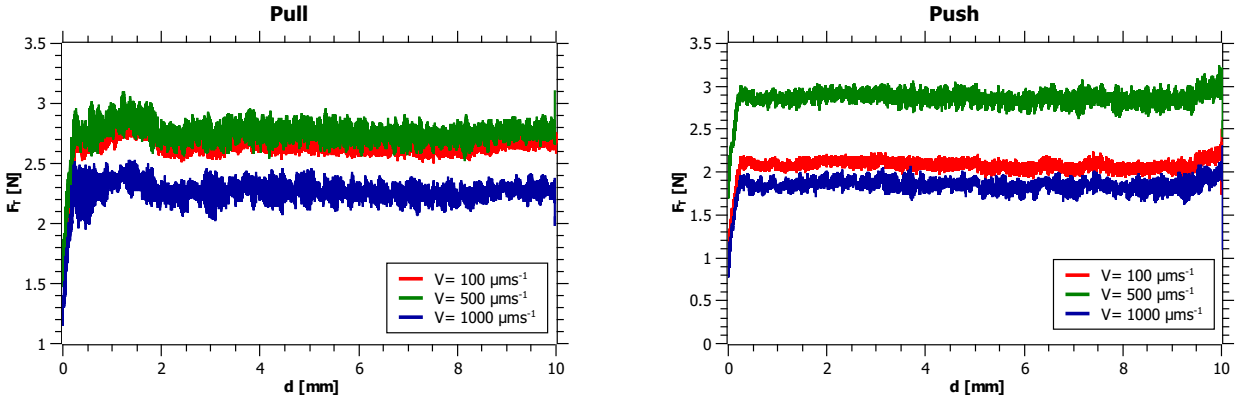

(a) (b)

Figure 8: Evolution of the tangential force occurring between the nitinol stent and the PTFE catheter versus displacement in (a) traction (pull) and in (b) compression (push) at $100 \mu m s^{-1}$ (smoothed with a 20 points adjacent averaging algorithm)

observed in the nitinol tube case, in spite of the same sampling rate and the same smoothing algorithm being used. Besides, noise is clearly reduced for compression measurements compared to the ones in traction, probably due to the reduction of stick-slip phenomena once the stent has been compressed. This stick-slip-like behaviour can be attributed to the stent mesh design, whose variations of local geometry are likely to evolve during the sliding velocities. Hence, any modification in stent design could lead to a change in the tribological behaviour. The latter is mainly dependent on the evolution of the real contact area during the sliding process. At this stage, one question remains which is "how does this real contact area evolve during the pushing and pulling tests?"

3.3 Evolution of the real contact area vs the sliding distance

The purpose, in a first step, is to measure the static real contact area generated by radial expansion of the stent within the PTFE catheter. This real contact can be measured by optical topographical analysis – by assessing the asperity slope analysis as proposed by Persson's theory [8] – as long as the tube is transparent enough to avoid light scattering that inevitably leads to measurement errors. Since the PTFE

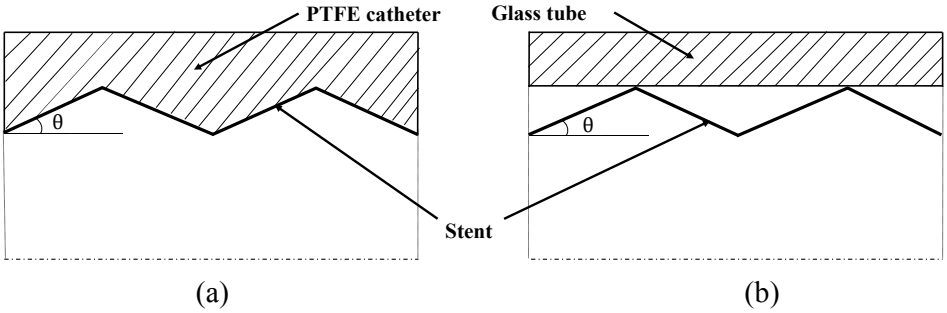

Figure 9: Schematic illustration of the contact behaviour (ie, slope angle θ) of a nitinol stent inserted within (a) a PTFE catheter and (b) a glass tube. For the PTFE material, the real contact is only controlled by the slope angle θ of the nitinol stent.

catheter does not have these optical properties, a glass tube displaying the same inner diameter has been used instead. As shown in figure 9 that displays a diagram of the setting, angle θ - which defines the asperity slope – is not really affected by the material change as long as the inner diameter of the catheter stays the same. Indeed, the catheter takes the form imposed by the expanded stent inside the volume because of the PTFE softness.

By means of Persson's theory, the real contact area is computed with the following relationships involving the mechanical $E^{'}$ and topographical $\Delta q = tan\theta$ properties of materials and the nominal contact pressure σ_0. It is worth noting that Persson's relationship (equation 1) is scale dependent by means of the magnification parameter ζ:

$$\frac{A_r(\zeta)}{A_0} = erf(\frac{\sigma_0}{E^{'}\Delta q}) \tag{1}$$

with A_r and A_0 being the real and nominal contact area. σ_0 and $E^{'}$ represents respectively the nominal pressure and the effective elastic modulus defined as follows:

$$\frac{1}{E^{'}} = \frac{1-\nu_{PTFE}^2}{E_{PTFE}} + \frac{1-\nu_{Nitinol}^2}{E_{Nitinol}} \tag{2}$$

with ν_α and E_α represents the Poisson's ratio and the Young's modulus of PTFE and Nitinol, respectively (α =[PTFE,Nitinol]). Considering the properties compiled in table 1, the effective elastic modulus is calculated to be 1452.3 MPa.

Figure 10a shows a typical view of the 2D topographical map of the stent within the glass tube. Using Gwyddion software, a representative square enlargement of figure 10b is obtained in order to define the normal contact area A_0 as suggested by Persson [8]. The square's side is chosen to be the same as the stent's strand width because it is the largest possible length in this discontinuous contact case (cf. Fig.10b). The root mean square slope Δq is then computed with Gwyddion by extracting an average profile on A_0 (cf. Fig.10b) as shown in Fig.10c. The latter is actually averaged on sixty individual profiles. Since $\Delta q(\zeta)$ is scale dependent too, its value has been computed for the highest magnification imposed by the image resolution. The averaged value $\overline{\Delta q}$ computed on eleven measures is about 8.37 ± 1.23. As a result, Fig.11 shows the evolution of the contact area ratio $\frac{A_r}{A_0}$ versus the contact pressure σ_0. As expected, the Persson's theory provides the evolution of the real contact from zero to full contact, i.e., when $A_r = A_0$:

- In the first part (red curve), the real contact area is proportional to the applied pressure, in agreement with other theories proposed by Greenwood and Williamson [9] and, Bush, Gibson and Thomas [10], for instance.

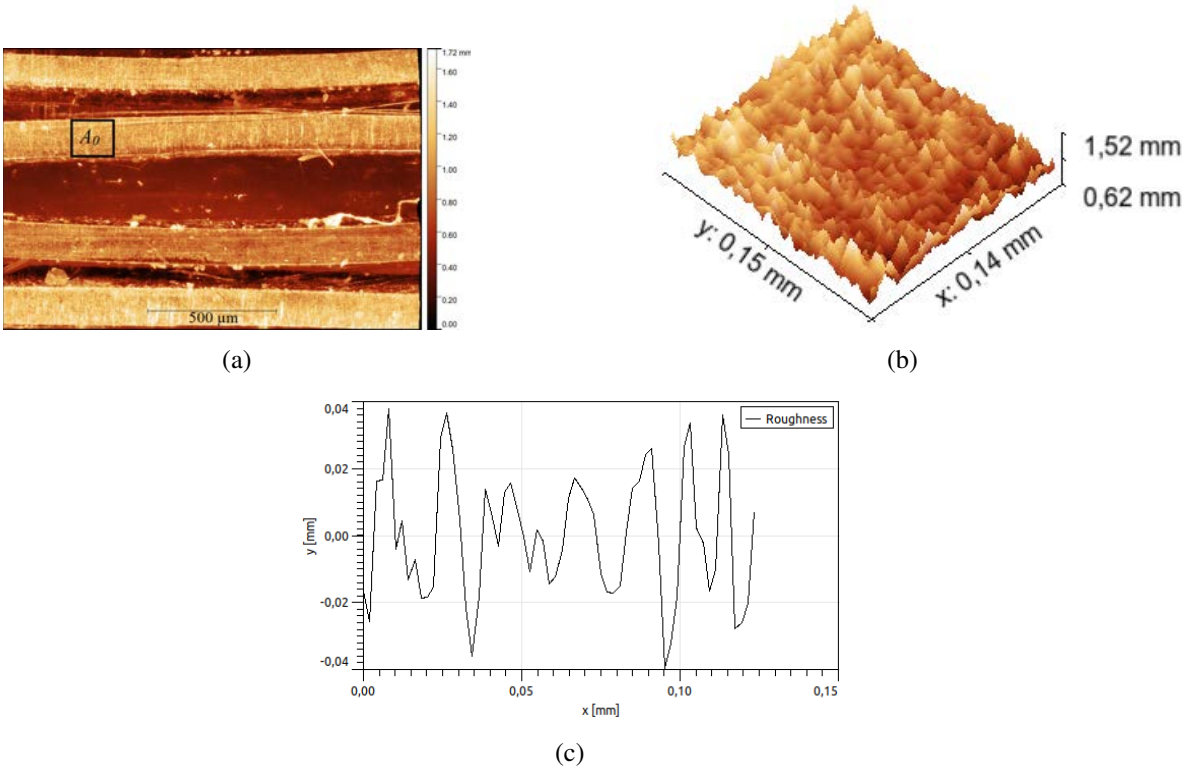

(a) (b)

(c)

Figure 10: (a) Typical 2D-topographical view of the nitinol stent within the glass tube ; (b) Enlargement of the nominal contact area A_0 extracted from figure 10a ; (c) Average roughness profile carried out on the whole surface picture (Fig.10b)

- In the second part (blue curve), the real contact area is no longer proportional to the contact pressure. The latter is specific to Persson's theory [8], as it well characterizes the contact behaviour of elastomers subjected to high loadings. It is worth mentioning that Persson's theory encompasses the linear and non-linear cases in a generalized relationship (cf. Eq. 1) [11].

The second step is to find the value of the average contact pressure σ_0 generated by the nitinol stent expansion within the PTFE catheter. For this purpose, X-Ray tomography is used as mentioned in section 2.3. As shown in figure 5a, the nitinol stent can be easily distinguished from the PTFE because its density is much greater than that the latter one ($\rho_{Nitinol} = 6.45\ g/cm^3$ and $\rho_{PTFE} = 2.2\ g/cm^3$). By measuring the deformation of the inner diameter ΔD of the PTFE catheter owing to the stent expansion - i.e, difference between the deformed diameter of the PTFE catheter due to stent expansion, measured by tomography, and its initial diameter D - (see values in figure 5a), the elastic coupling relationship (cf. Eq. 3) [12] allows the estimation of the average contact pressure σ_0, which depends only on the PTFE properties (cf Table 2). The average contact pressure was calculated to be 48 MPa.

$$\Delta D = \frac{\sigma_0 D^2}{2 w_t E} \tag{3}$$

Inserting σ_0 into Eq.1, the contact area ratio is in the order of 0.5% which is approximatively one-hundred times lower than the apparent surface ratio. The latter represents the area occupied by the stent in relation to the area of the glass tube shown in Fig.10a. Figure 11b shows a typical view of this real contact area obtained after vertical slicing, consisting of decreasing a binarization threshold on the stent's strands topographical view to have a discrete area of 0.5%. By considering the sliding direction (arrow

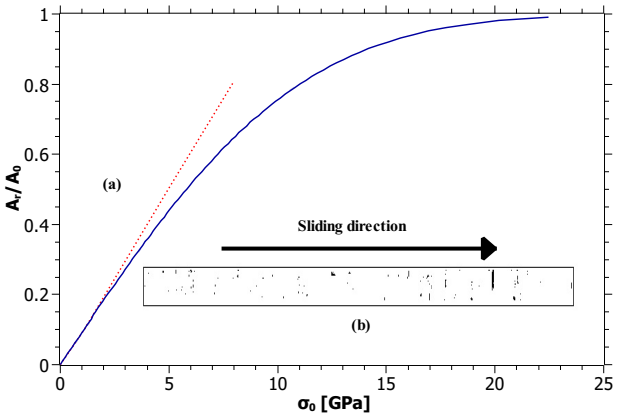

Figure 11: (a) Contact area ratio $\frac{A_r}{A_0}$ versus contact pressure σ_0 following the Persson's theory (b) Experimental view of the real contact area for $\frac{A_r}{A_0}$ = 0.5% corresponding to a contact pressure of σ_0 = 48 MPa

Table 2: PTFE catheter dimensions and properties

D (mm)	5
ΔD (mm)	0.41
E (MPa)	1200
w_t (mm)	0.5

in figure 11b), these discrete patterns strongly contribute to the stick-slip-like behaviour observed for the stent in figure 8.

Referring to figure 11a, this value corresponds to the linear part of the Persson's curve. According to Carbone et al. [11], in this peculiar case, the Persson's relationship can be simplified by expanding the error function (erf) to the first order to provide a direct relationship between A_r and F_N. It is worth mentioning that this one is only valid for small normal loads:

$$A_r = \frac{2}{\pi}\frac{1}{E'}\left(\frac{\pi}{\Delta q^2}\right)^{1/2} F_N \tag{4}$$

In order to compute the evolution of the real contact area as a function of displacement for different velocities in traction and compression, the different normal forces are connected to the stent tangential forces (cf. Fig.8) with the coefficients of friction (cf. Fig.7), which have been calculated from the nitinol/PTFE assembly, in traction and compression for every velocity (cf. Eq.5). In this case, the material part of the dissipation by friction of the stent and the tube is assumed to be the same via the friction coefficient. Hence, the dissipated part assessed by means of the variations of real contact area versus displacement only corresponds to the part associated with the design (topography) and is then completely decoupled from the materials one.

$$A_r = \frac{2}{\pi}\frac{1}{E'}\left(\frac{\pi}{\Delta q^2}\right)^{1/2} \frac{F_T(d)}{\mu} \tag{5}$$

Figure 12 shows the evolution of the real contact area versus stent displacement in traction and compression for three sliding velocities (computed by Eq.5 and data from Fig.7 and 8, respectively). As expected, the real contact area strongly fluctuates around an average value. The latter decreases with

the sliding velocity in pulling tests, whereas these fluctuations are less obvious in pushing ones because the stent compression hinders its own motion. Whatever the test velocity, the real contact area is always lower during pushing than pulling test.

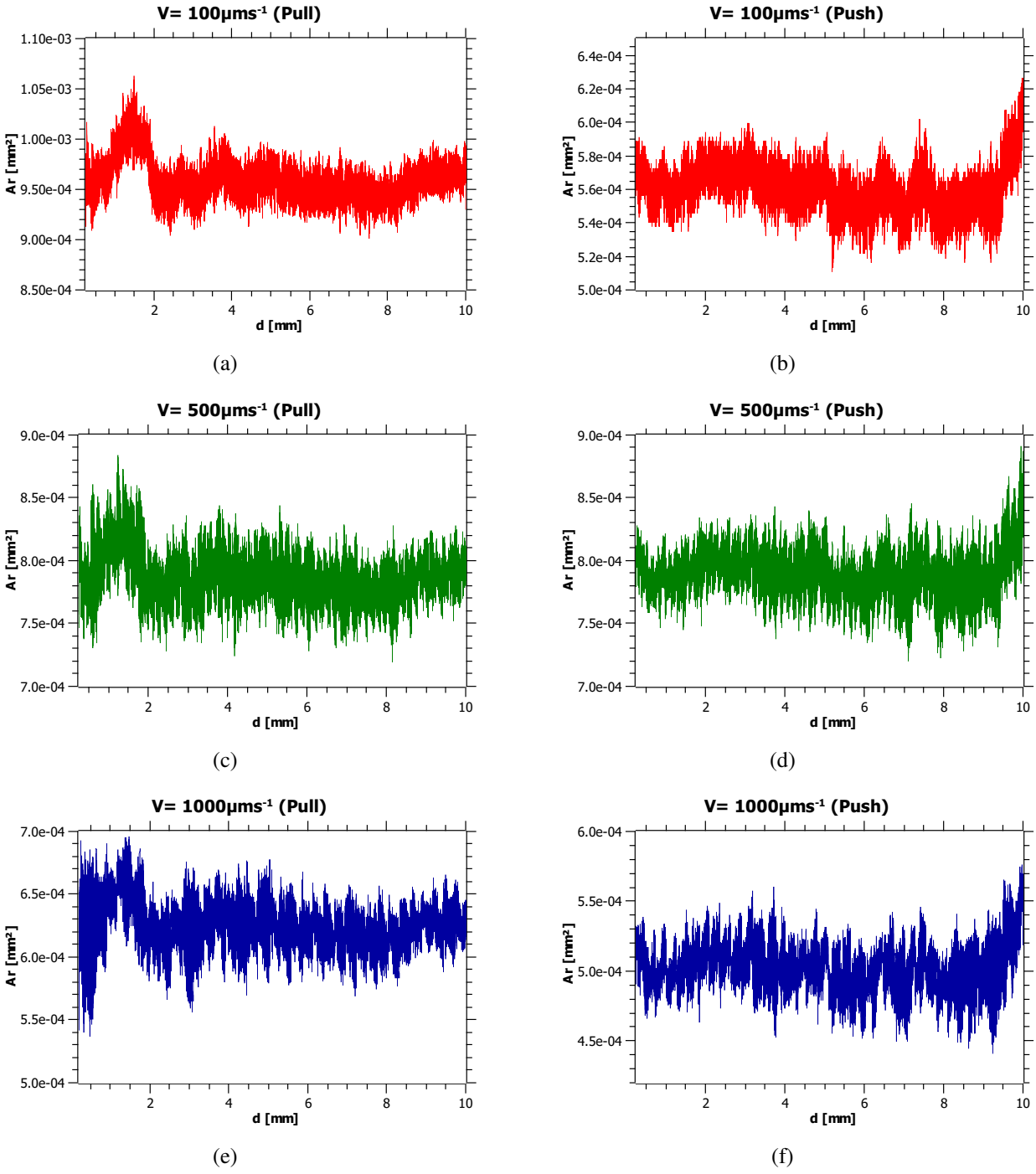

Figure 12: Evolution of the real contact area as a function of stent displacement in traction and compression for different velocities

Besides, the tangential stress τ at the interface between the PTFE catheter and nitinol stent can be computed by dividing the tangential force F_T by the real area at 0.5% (cf. Fig.13). It appears that the

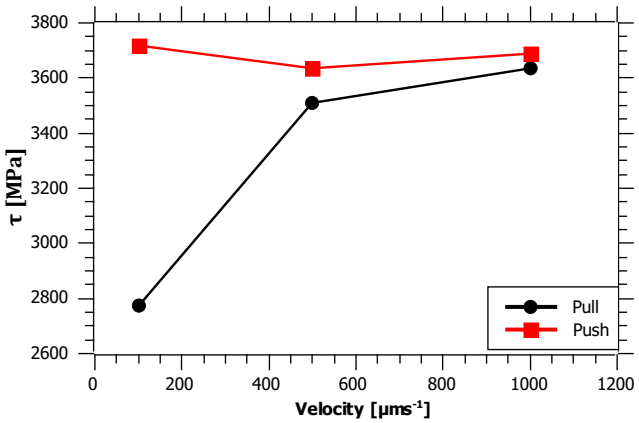

Figure 13: Evolution of the tangential stress at the interface between the stent and the PTFE catheter as function of imposed velocities for traction and compression (for the case of $\frac{A_r}{A_0} = 0.5\%$)

tangential stress is rather independent of the velocity in pushing tests, whereas it continuously increases with velocity in pulling tests. This evolution can be used to simplify numerical simulations of stent release behaviour as it implicitly integrates the design of the stent within the friction law. So, the complex geometry of a stent could be modelled by a simple tube displaying this complex frictional behaviour and distribute the tangential stress over the whole contact area. It is worth noting that any change in the stent geometry leads to alter the rigidity of its structure once compressed into the catheter and, therefore, modify the tangential stress at the interface. To know the latter for a new design, a topographical analysis is just needed, in addition to a new tribological test of stent within the catheter, to determine the corresponding root mean square slope.

4 Conclusion

In this study, the frictional behaviour of a nitinol stent sliding within a PTFE catheter has been characterised using an original multiscale method. First tribological tests in traction and compression have been carried out on a tensile testing machine to extract the frictional force occurring during the sliding of the nitinol stent within the PTFE catheter for various velocities. This evolution is combined with the material friction coefficient (obtained from sliding of a nitinol tube within the PTFE catheter) to lead to the variation of the real contact area with respect to the mechanical and topographical properties (i.e., depending on the stent design). The assessment of the dynamic real contact area finally allows to compute an equivalent tangential stress at the interface suitable for simplifying any numerical simulation of stent release. To bridge the gap between the friction force and the real contact area, a generic multi scale approach using topographical and tomographical analyses has been then specifically developed.

Acknowledgment

We would like to express our gratitude to the FEMTO-ST research institute, the CNRS, and the Plan France Relance for generously funding our research, enabling us to carry out this study and bring it to completion.

We also wish to acknowledge Stani Carbillet and the AMETISTE platform for granting us access to the tensile testing machine and the digital microscope, and Xavier Gabrion, and the MIFHySTO platform for providing us the opportunity to use the X-Ray tomography equipment.

References

[1] A. Sallami, W. Khalil, T. Bouraoui, and T. Ben Zineb, "A finite-strain thermomechanical behavior model for iron-based shape memory alloys accounting for coupling between phase transformation and plastic slip," *International Journal of Plasticity*, vol. 124, pp. 96–116, 2020.

[2] C. Cisse, W. Zaki, and T. Ben Zineb, "A review of constitutive models and modeling techniques for shape memory alloys," *International Journal of Plasticity*, vol. 76, pp. 244–284, 2016.

[3] W. Khalil, A. Mikolajczak, C. Bouby, and T. Ben Zineb, "A constitutive model for fe-based shape memory alloy considering martensitic transformation and plastic sliding coupling: Application to a finite element structural analysis," *Journal of Intelligent Material Systems and Structures*, vol. 23, no. 10, pp. 1143–1160, 2012.

[4] S. Vad, A. Eskinazi, T. Corbett, T. McGloughlin, and J. P. Vande Geest, "Determination of Coefficient of Friction for Self-Expanding Stent-Grafts," *Journal of Biomechanical Engineering*, vol. 132, no. 12, 2010, 121007.

[5] H. Onizuka, E. Sueyoshi, I. Sakamoto, and T. Miura, "Dilation of inferior vena cava and iliac veins in elite athlete," *Journal of Vascular Surgery: Venous and Lymphatic Disorders*, vol. 5, p. 575, 2017.

[6] A. Sallami, P. Malecot, F. Richard, M. Fontaine, A. Lejeune, S. David, P. Vescovo, C. Moureaux, and P. Stempflé, "The effect of heat treatment on the mechanical behavior of an ASTM-F2063 nitinol stent intended for venous application." in *E-Mrs - European Materials Research Society: Spring meeting*, Strasbourg, France, 2023.

[7] T. Connolley, D. Nash, J.-Y. Buffière, F. Sharif, and P. E. McHugh, "X-ray micro-tomography of a coronary stent deployed in a model artery," *Medical Engineering & Physics*, vol. 29, no. 10, pp. 1132–1141, 2007.

[8] B. Persson, "Contact mechanics for randomly rough surfaces," *Surface Science Reports*, vol. 61, no. 4, pp. 201–227, 2006.

[9] J. A. Greenwood and J. P. Williamson, "Contact of nominally flat surfaces," *Proceedings of the royal society of London. Series A. Mathematical and physical sciences*, vol. 295, no. 1442, pp. 300–319, 1966.

[10] A. Bush, R. Gibson, and T. Thomas, "The elastic contact of a rough surface," *Wear*, vol. 35, no. 1, pp. 87–111, 1975.

[11] G. Carbone and F. Bottiglione, "Asperity contact theories: Do they predict linearity between contact area and load?" *Journal of the Mechanics and Physics of Solids*, vol. 56, no. 8, pp. 2555–2572, 2008.

[12] F. Esnault, *Ingénierie mécanique: Tome 3*. Paris: DUNOD, 2019.